



Diagnostic Value of Axillary Ultrasound, MRI, and ¹⁸F-FDG-PET/CT in Determining Axillary Lymph Node Status in Breast Cancer Patients

AYŞEGÜL AKTAŞ¹, MERYEM GÜNAY GÜRLEYİK¹, SİBEL AYDIN AKSU², FUGEN AKER³, SERKAN GÜNGÖR⁴

¹Department of General Surgery, İstanbul Haydarpaşa Numune Training and Research Hospital, University of Health Sciences Turkey, İstanbul, Turkey

²Department of Radiology, İstanbul Haydarpaşa Numune Training and Research Hospital, University of Health Sciences Turkey, İstanbul, Turkey

³Department of Pathology, İstanbul Haydarpaşa Numune Training and Research Hospital, University of Health Sciences Turkey, İstanbul, Turkey

⁴Department of Nuclear Medicine, Göztepe Training and Research Hospital, İstanbul Medeniyet University, İstanbul, Turkey

ABSTRACT

Objective: Knowing axillary lymph node (ALN) status before surgery affects decisions about treatment modalities. Therefore, reliable, noninvasive diagnostic methods are important for determining ALN metastases. We aimed to accurately evaluate the patient's ALN status with noninvasive imaging modalities while making treatment decisions.

Materials and Methods: Patients who received the axillary ultrasound (AUS), magnetic resonance imaging (MRI), or ¹⁸F-fluorodeoxyglucose positron emission tomography/computed tomography (¹⁸F-FDG-PET/CT) imaging modalities and whose ALNs were confirmed histopathologically by fine needle aspiration cytology (FNAC), sentinel lymph node biopsy (SLNB), or ALN dissection (ALND) were included in the study.

Results: The sensitivity, specificity, positive predictive value (PPV), negative predictive value (NPV), and accuracy of AUS for the detection of ALN metastases were 83%, 62%, 59.2%, 54.8%, and 79.1%, respectively. For MRI they were 86.1%, 75%, 68.5%, 51.6%, and 85.3%, respectively, and for ¹⁸F-FDG-PET/CT they were 78%, 53%, 56.2%, 51.4%, and 72.5%, respectively. ALNs were found to be metastatic in all patients who were reported positive in all three imaging modalities. ALN metastases were detected in 19 of 132 patients (false negativity, 14.3%) in whom AUS, MRI, and ¹⁸F-FDG-PET/CT images were all reported as negative.

Conclusion: In our study, we found that the diagnostic performance of MRI was slightly better than AUS and ¹⁸F-FDG-PET/CT. When we used imaging modalities together, our accuracy rate was better than when we used them alone. For accurate evaluation of axillary lymph nodes, imaging modalities should be complementary rather than competitive.

Keywords: ¹⁸F-FDG-PET/CT, Axillary lymph node metastases, axillary ultrasound, diagnostic performance, MRI, Sentinel lymph node biopsy

Cite this article as: Aktaş A, Gürleyik MG, Aydın Aksu S, Aker F, Güngör S. Diagnostic Value of Axillary Ultrasound, MRI, and ¹⁸F-FDG-PET/CT in Determining Axillary Lymph Node Status in Breast Cancer Patients. Eur J Breast Health 2022; 18(1): 37-47

Key Points

- The status of the axillary lymph nodes is one of the most important prognostic factors in patients with breast cancer.
- Axillary lymph node evaluation is the crucial step for treatment decision in newly diagnosed breast cancer.
- Imaging modalities can be used to accurately determine the status of axillary lymph nodes.
- False negativity rates are the most important deficiency of imaging modalities such as axillary ultrasound, MRI, ¹⁸F-FDG-PET/CT.

Introduction

Despite advances in breast cancer management, axillary lymph node (ALN) status remains the most important prognostic factor in terms of staging, treatment, prognosis, recurrence, and survival. In a 10-year follow-up, ALN metastasis at the time of diagnosis in breast cancer increased the risk of recurrence (1, 2). Until recently, axillary lymph node dissection (ALND) was standard in breast cancer patients with clinically suspected ALNs, or cytologically proven axillary metastasis following ultrasound-guided fine needle aspiration cytology (FNAC) at the time of diagnosis or after neoadjuvant chemotherapy (NAC) (3, 4).

ALND gives precise information about the nodal burden, but due to the associated morbidities, particularly seroma and lymphedema, the less invasive method of sentinel lymph node biopsy (SLNB) is now standard in patients with clinically negative ALNs (3, 5). In addition, the International Breast Cancer Study Group (IBCSG) 23-01 study, which included patients with micrometastatic SLNB, found no significant difference in disease-free survival at 5-years of follow-up (5, 6). Similarly, in the American College of Surgeons Oncology Group (ACOSOG) Z0011 study in patients for whom only breast conservative surgery (BCS) and whole breast radiotherapy (RT) were performed, and ≤ 2 macrometastatic SLNB patients with or without ALND were compared, no significant differences were found in terms of disease-free survival during approximately 5 years of follow-up (7). In the AMAROS study, initiated by the European Organization for Research and Treatment of Cancer (EORTC), patients with clinically negative ALN, T1 or T2 stage breast cancer, and micro- or macrometastatic SLNB, no difference was found between the groups treated with ALND or axillary radiotherapy during five years of follow-up in terms of local recurrence and survival. In addition, less morbidity was found in the axillary radiotherapy group (5, 8).

However, SLNB is also invasive, and may have undesirable consequences. Therefore, the requirement for SLNB in the radiologically negative axilla in breast cancer has been investigated in many studies (Sentinel node vs. Observation after axillary Ultrasound (SOUND) and Intergroup-Sentinel-Mamma (INSEMA)-Trial-GBG 75) (9-11). This has encouraged reassessment of the role of imaging modalities for ALN staging (4).

Knowing ALN status before surgery affects decisions about treatment modalities. Therefore, reliable, non-invasive diagnostic methods are important for determining ALN metastases (1, 2). The aim of our study was to evaluate the diagnostic value of axillary ultrasound (AUS), magnetic resonance imaging (MRI), and ^{18}F -fluorodeoxyglucose-positron emission tomography/computed tomography (^{18}F -FDG-PET/CT) in determining ALN status in breast cancer patients with and without NAC compared to the gold standard of pathohistological or cytologic findings.

Materials and Methods

Study Design

Patients diagnosed with breast cancer and treated at the University of Health Sciences, Turkey, İstanbul Haydarpaşa Numune Training and Research Hospital, between January 2015 and December 2019, were retrospectively evaluated. In the daily practice of our clinic, AUS is routinely performed in the evaluation of axillary metastasis in patients with breast cancer. MRI is used to evaluate whether breast cancer is multicentric or not, and, notably, ^{18}F -FDG-PET/CT is used in the evaluation of distant metastasis. Of the 528 patients, a total of 336 patients who underwent AUS, MRI, and ^{18}F -FDG-PET/CT imaging were included. Patients who did not receive the AUS, MRI, or ^{18}F -FDG-PET/CT imaging modalities and whose ALNs were not confirmed histopathologically or cytopathologically by FNAC, SLNB, or ALND were not included in the study. Patients with distant metastases at the time of diagnosis were also excluded. Since the axillae of these 336 patients were evaluated retrospectively, AUS, MRI, and ^{18}F -FDG-PET/CT evaluations were reviewed, blinded to the other findings and investigators had no information about the final pathological ALN status.

Since axillary metastases may be eradicated with chemotherapy, and hence lack reference standard for axillary surgery, patients who received NAC were not included in the surgery group. The patients were categorized into two groups: patients who received NAC (NAC group, 100 patients) and those who underwent surgery after diagnosis (upfront surgery group, 236 patients). In the upfront surgery group, the axilla was evaluated according to the SLNB/ALND results, and in the NAC group, the axilla was evaluated according to the FNAC results. Primary tumor and ALN sizes were determined according to the largest radiological size in the NAC group and were evaluated according to the results of the surgical specimens in the upfront surgery group. With the results of SLNB or ALND in 236 patients in the upfront surgery group, patients with metastatic ALNs were grouped as 'metastatic', and patients with benign ALNs were grouped as 'benign'. According to the surgical specimen results of the upfront surgery group, ALN metastasis diameter and number were recorded. Micrometastatic nodes were defined as 0.2–2 mm as per the seventh edition of the American Joint Committee on Cancer breast cancer stage classification, published in 2010. In addition, isolated tumor cells in a sentinel node (<0.2 mm) were defined as node negative (12). Of 117 patients with FNAC results, there were 100 patients in the NAC group and 17 in the upfront surgery group. In the upfront surgery group, the FNAC results were compared to the SLNB and ALND results. According to FNAC results, patients with metastatic ALNs were grouped as 'metastatic', and patients with benign ALNs were grouped as 'benign'. Insufficient samples were not included in the FNAC results.

This study was approved by the local ethics committee (decision no: TUEK-771/04/2020).

AUS Protocol

Different US systems were used for the axillary US examinations by radiologists with variable years of experience. AUS was performed using a linear array transducer, in the supine oblique position, with the patient's hand above her head, with the arm abducted and externally rotated. ALNs were considered metastatic on US in the presence of any of the following criteria: loss or disruption of the central fatty hilum; loss or compression of the hyperechoic medullary region; parenchymal cortical thickness >3 mm; asymmetric cortical thickening; left-to-right asymmetry; round morphology (Solbiati Index <2); loss of the pericapsular fat line or irregular outer margins; the relationship with neighboring lymph nodes; and presence of increased peripheral blood flow. In the absence of these criteria, ALNs were considered negative for metastasis (Figure 1).

MRI Protocol

Breast MRI was performed on a 1.5T scanner using a dedicated 16-channel double-breast coil covering both breasts in the prone position (GE Optima 360 Bamboo: General Electric, Milwaukee, WI, USA). Gadobutrol (Gadovist[®], Bayer Health Care, Germany) was automatically injected as contrast agent through a catheter in the antecubital vein at 0.1 mmol/kg, followed by a saline flush. In the axial plane, T1-weighted FSE images (TR/TE, 677/5.6; matrix, 352 × 192; slice thickness, 5 mm) and T2-weighted FSE images (TR/TE, 6682/104; matrix, 256 × 256; slice thickness, 5 mm) were obtained. Dynamic, contrast-enhanced MRI examination included one pre- and five post-contrast images with bilateral axial acquisition using fat-suppressed T1-weighted imaging. Subtraction images and three-dimensional maximum intensity projection images were generated

for all studies. Diffusion-weighted imaging was also performed. MRI findings indicating lymph node metastases included the following: a short-axis diameter >5 mm; a maximal cortical thickness >3 mm; round shape; eccentric cortical thickening; and loss or compression of the fatty hilum. Both axillae were evaluated at the same time, and the ALNs ipsilateral to the breast cancer were compared to the contralateral nodes. If there were no differences in number, size, or shape between the ipsilateral and contralateral ALNs, they were recorded as negative. ALN was considered positive when one or more suspicious MRI findings were noted. Radiologists with varying years of experience evaluated the pretreatment MRI findings (Figure 2).

¹⁸F-FDG-PET/CT Protocol

All patients fasted for at least four hours before ¹⁸F-FDG administration. When the blood glucose was <11 mmol/L, 5–6 MBq ¹⁸F-FDG per kilogram of body weight was intravenously administered. ¹⁸F-FDG-PET/CT scans were carried out approximately 60 minutes after ¹⁸F-FDG administration using an integrated Philips Gemini TF model PET/CT scanner system (Philips Medical Systems, Cleveland, Ohio, USA). No additional contrast agent containing iodine was used for CT. PET/CT images were obtained from the head to the proximal thighs. Prior to PET acquisition, helical CT was performed under shallow breathing conditions using a low-dose CT protocol for attenuation map. PET images were reconstructed using CT for attenuation

correction with an ordered subset expectation maximization iterative reconstruction algorithm (Figure 3). We considered a ≥ 1.2 maximum standardized uptake value (SUV_{max}) a positive ALN (as used in the clinic), and an SUV_{max} value <1.2 and reactive designation were accepted as negative.

Statistical Analysis

Analyses of the data were performed using the statistical software package SPSS, version 24.0 (IBM Corp., Armonk, NY, USA). Descriptive statistics are presented as numbers and percentages for categorical variables, and mean, standard deviation, minimum, and maximum for numerical variables. The Student’s t-test was used to compare demographic parameters. The Kruskal-Wallis test was used to compare quantitative variables that did not show a normal distribution. A Bonferroni correction and Tukey test were used to compare quantitative variables that did not show a normal distribution between more than two groups. The Pearson correlation coefficient method was used for correlations. Diagnostic screening tests including sensitivity, specificity, positive predicted value (PPV), negative predicted value (NPV), and kappa compliance tests were used to determine the compatibility between qualitative data. The statistical significance level was at 95% confidence intervals, and $p < 0.05$ was considered significant.

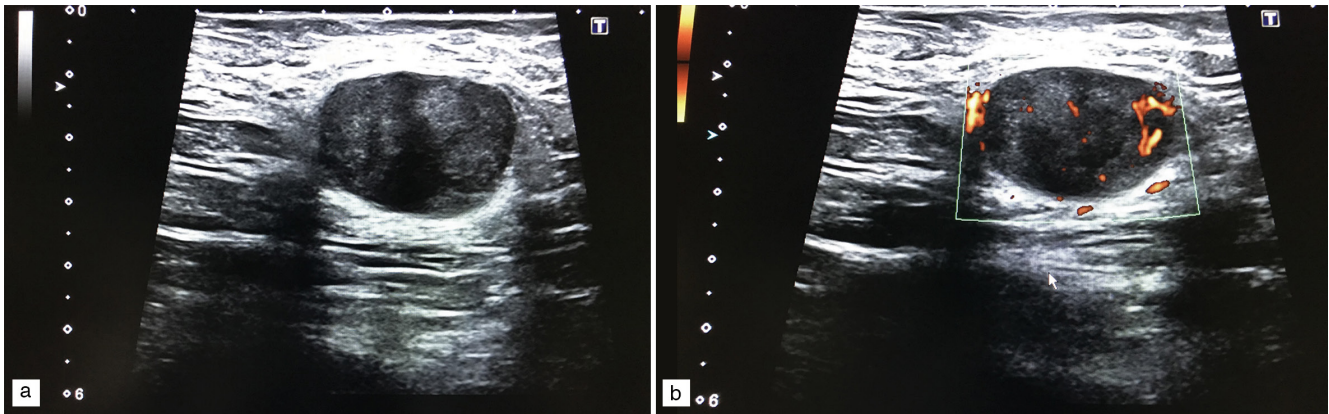


Figure 1. Human epidermal growth factor receptor 2 (+), Invasive ductal carcinoma in a 45-year-old woman with ipsilateral axillary lymph node metastasis. (a) B-mode sonogram shows an enlarged, round shaped lymph node with loss of the central fatty hilum in the left axillary fossa. (b) Power Doppler Sonogram reveals increased peripheral blood flow signals

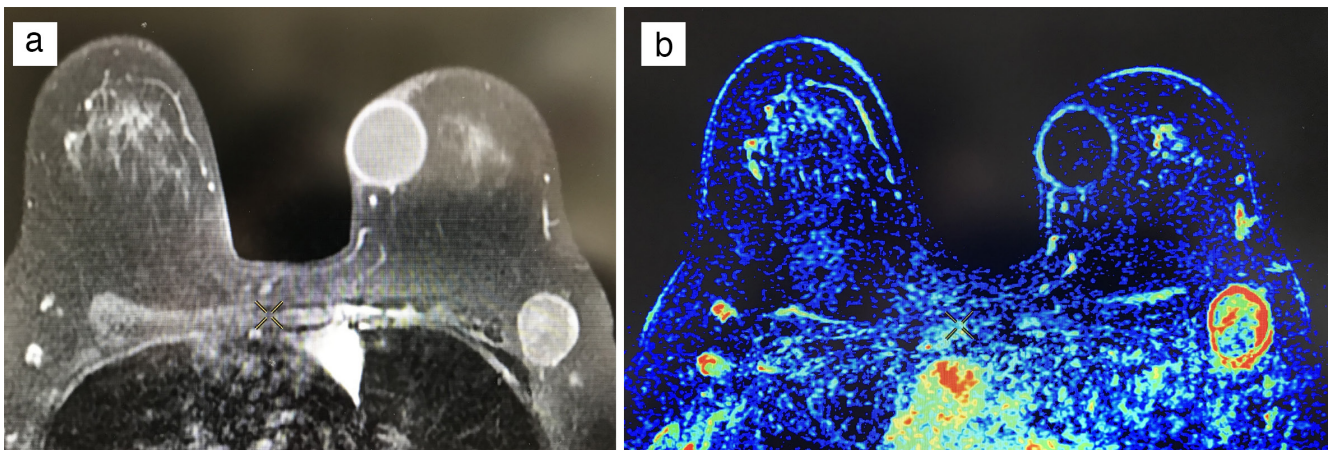


Figure 2. Dynamic contrast-enhanced magnetic resonance imaging examination of the same patient mentioned in Figure 1. (a) Contrast enhanced fat-suppressed T1-weighted axial image shows peripherally enhanced, round shaped left axillary lymph node with diameter of 38 × 22 mm. (b) Postcontrast subtracted axial image emphasizes rim-like contrast enhancement

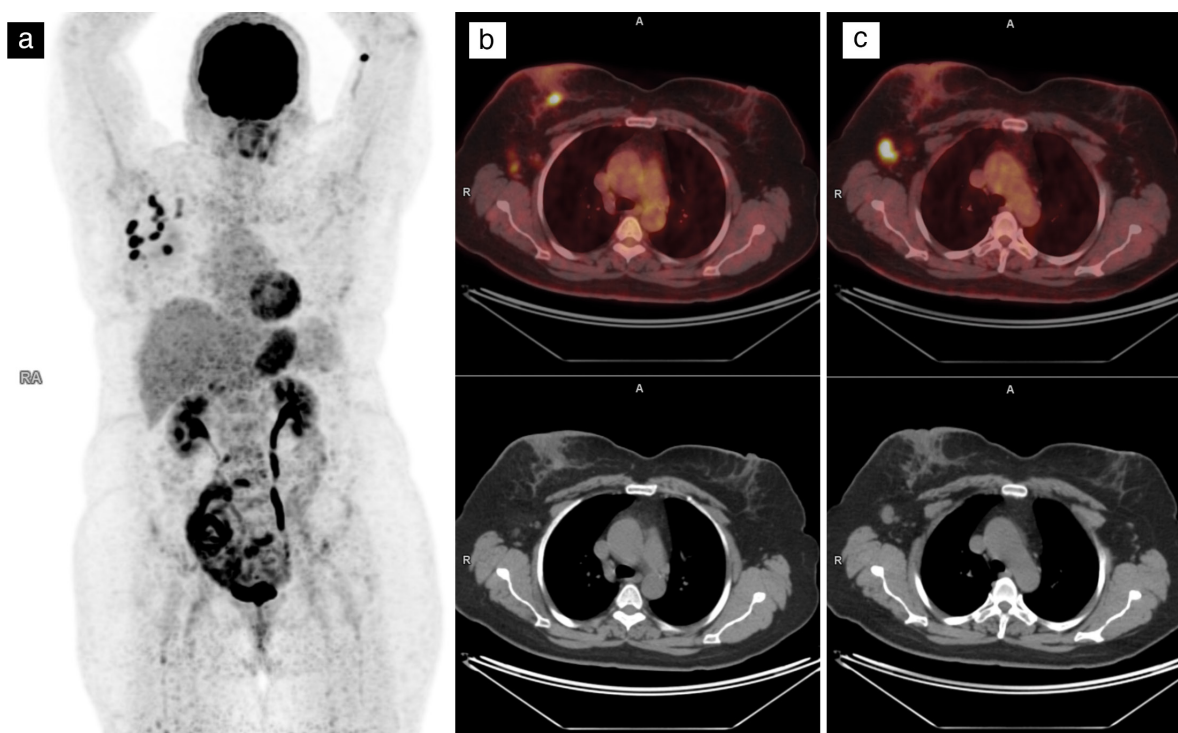


Figure 3. Invasive ductal carcinoma in a 49-year-old woman. (a) Maximum intensity projection positron emission tomography (PET) image demonstrates invasive ductal carcinoma in the right breast and multiple metastases in the right axillary lymph nodes. (b) Axial fused positron emission tomography-computed tomography (PET/CT), and CT show an intensely hypermetabolic focus [maximum standardized uptake value (SUV_{max}), 9.4] in the right retroareolar region with diameter of 12 x 11 mm, corresponding to the breast tumor. (c) Axial fused PET/CT, and CT reveal a metastatic axillary lymph node with high fluorodeoxyglucose (FDG) uptake (SUV_{max}: 10.7)

Results

The patients were categorized into two groups: patients who received NAC, and those who underwent surgery after diagnosis. Of the 336 patients, there were 100 in the NAC group and 236 in the upfront surgery group. The mean \pm standard deviation (SD) age was 50.1 \pm 11.8 years (range: 18–84). The mean \pm SD primary tumor size was 26.1 \pm 12.7 mm (range: 6–80 mm), and the mean \pm SD ALN size was 14.2 \pm 6.5 mm (range: 5–46 mm) (Table 1). When the two groups were compared, age was significantly younger in the NAC group ($p = 0.047$). There was no significant difference between tumor size and ALN size ($p = 0.187$, $p = 0.113$, respectively) (Table 1). A total of 172 tumors (51.1%) were located in the left breast. Tumor sizes were clinically categorized into four groups: cT1: <20 mm; cT2: 20–50 mm; cT3: >50 mm; cT4: invasion. Of these, 173 cases (51.4%) were cT2. ALN clinical findings on physical examinations of the patients were divided into three groups: cN0: non-palpable, cN1: mobile, and cN2: fixed. Of them, 165 cases (49.1%) were cN1. According to the results of histopathological evaluation, most patients (75%, 252 patients) had invasive ductal breast cancer (IDC), and 26 patients (7.7%) had invasive lobular carcinoma (ILC) in breast. On immunohistochemical profiling, out of 336 patients, 89 patients (26.4%) were Luminal A, 144 patients (42.8%) were Luminal B, HER2 (-), 42 patients (12.5%) were Luminal B, HER2 (+), 30 patients (8.9%) were HER2 (+), and 31 patients (9.2%) were TN (Table 2). When FNAC, SLNB, and ALND specimen results were evaluated histo- or cyto-pathologically, ALNs were metastatic in 188 patients (55.9%). Clinical and pathological characteristics of the patients in the upfront surgery group and NAC group are given separately in Table 2. In the NAC group, evaluated by FNAC, 90 of 100 patients had metastatic and 10

had benign ALNs. Upfront surgery patients were categorized into four groups according to the diameter of ALN metastases: no metastasis or isolated tumor cells, ≤ 2 mm, 3–9 mm, and ≥ 10 mm, respectively. In these 236 patients, the mean \pm SD ALN metastasis diameter was 3.84 \pm 5.94 mm (median: 0 mm, range: 0–40 mm), and no metastases were detected in 138 patients (58.5%). The mean \pm SD positive ALN metastasis diameter was 9.06 \pm 6.16 mm (median: 9 mm, range: 0.2–40 mm) in 98 patients. Metastases were ≤ 2 mm in 13 patients (5.5%), 3–9 mm in 44 patients (18.6%), and ≥ 10 mm in 41 patients (17.3%). Again, in the upfront surgery group, when the pathological ALN number (pN) was evaluated, it was categorized into four groups: pN0, benign; pN1, 1–3; pN2, 4–9; and pN3, ≥ 10 metastatic ALNs. In the upfront surgery group, 98 patients (41.5%) had metastatic ALNs. In all, 66 patients (27.9%) were pN1, 23 patients (9.7%) were pN2, and nine patients (3.8%) were pN3 (Table 2). In breast surgery, 149/236 patients (63.2%) underwent BCS, and 87/236 patients (36.8%) underwent mastectomy. In the upfront surgery group, direct ALND was performed on 35 patients (13.5%) in the evaluation of the axilla for staging. There were 138 patients (58.4%) who received SLNB/ALND and were reported as benign. SLNB followed by ALND was performed in 14.8% of patients (35 patients) and ≤ 2 metastatic ALNs were detected. In 3.8% of patients ($n=9$), ALND was performed following SLNB and ≥ 3 metastatic ALNs were detected. As in the ACOSOG Z0011 study, there were 22 patients (9.3%) who underwent BCS alone, had scheduled radiotherapy, and had ≤ 2 macrometastatic SLNs, and no further ALND.

In AUS, ALNs were determined to be positive in 181 cases (53.9%), and negative in 155 cases (46.1%). On histopathological examination, ALN metastases were found in 188 cases (56%), with

benign ALNs in 148 cases (44%). The accuracy of AUS in showing ALN status was 79.1%. ALNs were positive in 155 cases (46.1%) on MRI and ¹⁸F-FDG-PET/CT, while ALNs were determined to be negative in 181 cases (53.9%). The accuracy of MRI and ¹⁸F-FDG-PET/CT in showing ALN status was 85.3% and 72.5%, respectively (Table 3). When evaluated by receiver operating characteristics curve analyses, the area under the curve (AUC) was 0.851 for ALN SUV_{max}.

In cases where AUS, MRI and ¹⁸F-FDG-PET/CT were false negative in the upfront surgery group, the mean ALN metastasis diameters were 3.73 (range: 0.2–9) mm, 3.54 (range: 0.2–10) mm, and 4.56 (range: 0.2–12) mm, respectively (Table 4). ALNs of the patients in whom AUS, MRI, and ¹⁸F-FDG-PET/CT images concordantly were reported as positive were also found to be metastatic according to the FNAC, SLNB, and ALND results. ALN metastases were detected in 19 of 132 patients (all upfront surgery group) (14.3%) in whom AUS, MRI, and ¹⁸F-FDG-PET/CT images concordantly were reported as negative. Mean ALN metastasis diameter was 3.27 (range: 0.2–9) mm (Table 5), and only one patient was pN2 (Table 6).

The sensitivity, specificity, PPV, NPV, and accuracy of AUS for the detection of ALN metastases were 83%, 62%, 59.2%, 54.8%, and 79.1%, respectively. For MRI these values were 86.1%, 75%, 68.5%, 51.6%, and 85.3%, respectively, and for ¹⁸F-FDG-PET/CT they were 78%, 53%, 56.2%, 51.4%, and 72.5%, respectively. Kappa correlation

levels between ALN positivity and AUS, MRI, and ¹⁸F-FDG-PET/CT results were 67.3%, 77.5%, and 60.5%, respectively (Table 3).

Discussion and Conclusion

ALN staging is an important step in the evaluation of newly diagnosed breast cancer patients. Knowing the presence of metastatic ALN involvement in clinically node-negative or node-positive patients is important in their treatment (12).

Radiological staging of ALN is performed with AUS, MRI, and ¹⁸F-FDG-PET/CT. AUS is widely used in the evaluation of ALN status in breast cancer because it is easy to perform, inexpensive, does not involve radiation, and is noninvasive (1). AUS is an operator-dependent modality for ALN metastases, so that reported sensitivity and specificity are variable and controversial (13). However, its accuracy for evaluating ALN metastases depends on the size of the ALNs. In the case of cN0, small ALN or metastasis diameter, the overall sensitivity of AUS is 56%–75%, and specificity is 70%–90% (14). In the upfront surgery group, the mean ALN metastasis diameter of our false-negative patients on AUS was 3.73 mm. In addition, AUS allows image-directed needle biopsy. In morphological evaluations, AUS alone has insufficient sensitivity and low PPV, and if ALN metastasis is suspected, AUS-guided FNAC is recommended and enables ALNs to be evaluated more accurately (15, 16).

Table 1. Comparison of means of patients' variables with and without NAC and ALN metastases

	ALN	n	Mean ± SD	Min-max	p-value
Age (year)		336	50.1±11.8	18–84	
	Metastatic	188	29.6±13.8	8–80	
Tumor size (mm)	Benign	148	21.6±9.5	6–53	0.007
	Total	336	26.1±12.7	6–80	
ALN size (mm)	Metastatic	188	16.5±7	7–46	0.001
	Benign	148	11.4±4.4	5–30	
ALN SUV _{max}	Total	336	14.2±6.5	5–46	0.037
	Metastatic	188	4.54±4.9	0–24.9	
Ki-67 level	Benign	148	0.2±0.7	0–4	0.008
	Total	336	2.6±4.3	0–24.9	
	Metastatic	188	31.4±19.5	2–90	
	Benign	148	25.5±20.5	2–90	
	Total	336	28.8±20.2	2–90	
	NAC group (n=100)		Upfront surgery group (n=236)		
	Mean ± SD	Min-max	Mean ± SD	Min-max	p-value
Age (year)	43.4±8.7	18–66	52.8±11.8	24–84	0.047
Tumor size (mm)	33.2±13.4	9–80	23.2±11.2	6–72	0.187
ALN size (mm)	18.2±7.5	8–41	12.6±5.3	5–46	0.113
ALN SUV _{max}	5.5±4.9	0–22.4	1.4±3.3	0–24.9	0.042
Ki-67 level	35.3±19.8	2–90	26.1±19.7	2–90	0.031

NAC: Neoadjuvant chemotherapy, ALN: Axillary lymph nodes, SD: Standard deviation, Min: Minimum, Max: Maximum, mm: Millimeter, ALN SUV_{max}: Axillary lymph nodes maximum standardized uptake value, n: Number

Table 2. Clinical and pathological characteristics of the patients

		Upfront surgery group (n=236)		NAC group (n=100)		p-value	Total (n=336)	
		n	%	n	%		n	%
ALN	Metastatic	98	41.5	90	90	0.052	188	55.9
	Benign	138	58.5	10	10		148	44.1
cT	cT1: ≤20 mm	110	46.6	16	16	0.769	126	37.5
	cT2: 20–50 mm	115	48.7	58	58		173	51.4
	cT3: >50 mm	9	3.8	8	8		17	5.1
	cT4: invasion	2	0.8	18	18		20	5.9
cN	cN0: non-palpable	149	63.1	8	8	0.049	157	46.7
	cN1: mobile	81	34.3	84	84		165	49.1
	cN2: fixed	6	2.5	8	8		14	4.2
Histopathological types	IDC	170	72	82	82	0.882	252	75
	ILC	18	7.6	8	8		26	7.7
	IDC + ILC	5	2.1	0	0		5	1.4
	Others	43	18.2	10	10		53	15.7
Luminal subtypes	A	80	33.9	9	9	0.031	89	26.4
	B, HER2 (-)	101	42.8	43	43		144	42.8
	B, HER2 (+)	21	8.9	21	21		42	12.5
	HER2 (+)	18	7.6	12	12		30	8.9
	TN	16	6.8	15	15		31	9.2
AUS	Positive	81	34.3	100	100	0.001	181	53.8
	Negative	155	65.6	0	0		155	46.1
MRI	Positive	70	29.7	85	85	0.038	155	46.1
	Negative	166	70.3	15	15		181	53.8
¹⁸ F-FDG-PET/CT	Positive	70	29.7	85	85	0.127	155	46.1
	Negative	166	70.3	15	15		181	53.8
pN	pN0: benign	138	58.4					
	pN1: 1–3	66	27.9					
	pN2: 4–9	23	9.7					
	pN3: ≥10	9	3.8					
ALN metastasis diameter (mm)	1: 0	138	58.4					
	2: ≤2 mm	13	5.5					
	3: 3–9 mm	44	18.6					
	4: ≥10 mm	41	17.3					
Breast surgery	BCS	149	63.2					
	Mastectomy	87	36.8					
Axillary surgery	BCS + ALND	35	14.8					
	BCS + SLNB	114	48.3					
	Mastectomy +ALND	44	18.6					
	Mastectomy + SLNB	43	18.2					

NAC: Neoadjuvant chemotherapy, ALN: Axillary lymph nodes, cT: Clinical tumor, mm: Millimeter, cN: Clinical node, IDC: Invasive ductal carcinoma, ILC: Invasive lobular carcinoma, HER2: Human epidermal growth factor receptor 2, TN: Triple negative, AUS: Axillary ultrasound, MRI: Magnetic resonance imaging, ¹⁸F-FDG-PET/CT: ¹⁸F-Fluorodeoxyglucose positron emission tomography/computed tomography, pN: Pathological node, BCS: Breast conserving surgery, ALND: Axillary lymph node dissection, SLNB: Sentinel lymph node biopsy, n: Number

Table 3. Diagnostic performance of imaging modalities in detecting the axillary lymph nodes metastases

		AUS		MRI		¹⁸ F-FDG-PET/CT	
		n	%	n	%	n	%
ALN (+), radiological (+) (true positive)	Upfront surgery group	67	19.9	67	19.9	57	16.9
	NAC group	90	26.7	85	25.2	81	24.1
	Total	157	46.7	152	45.2	138	41.1
ALN (-), radiological (+) (false positive)	Upfront surgery group	14	4.1	3	0.8	13	3.8
	NAC group	10	2.9	0	0	4	1.1
	Total	24	7.1	3	0.8	17	5.1
ALN (-), radiological (-) (true negative)	Upfront surgery group	124	36.9	135	40.1	125	37.2
	NAC group	0	0	10	2.9	6	1.7
	Total	124	36.9	145	43.1	131	38.9
ALN (+), radiological (-) (false negative)	Upfront surgery group	31	9.2	31	9.2	41	12.2
	NAC group	0	0	5	1.4	9	2.6
	Total	31	9.2	36	10.7	50	14.8
Sensitivity		83		86.1		78	
Specificity		62		75		53	
PPV		59.2		68.5		56.2	
NPV		54.8		51.6		51.4	
Accuracy		79.1		85.3		72.5	
Kappa		67.3		77.5		60.5	

AUS: Axillary ultrasound, MRI: Magnetic resonance imaging, ¹⁸F-FDG-PET/CT: ¹⁸F-Fluorodeoxyglucose positron emission tomography/computed tomography, ALN: Axillary lymph nodes, NAC: Neoadjuvant chemotherapy, PPV: Positive predicted value, NPV: Negative predicted value, n: Number

Breast MRI is frequently used because, like AUS, it is non-invasive and does not use radiation (17). The main advantage of MRI is that it provides anatomical information about the breast and axilla. It is used to evaluate the distance of the primary tumor to the skin, pectoral muscle, and areola, the local regional areas, and the contralateral breast (3, 18, 19). In addition, it has high sensitivity for detecting additional lesions that cannot be detected by ultrasound or mammography (17, 20). The role of MRI in determining ALN metastases has shown moderate sensitivity and low-medium specificity (16). In our study, sensitivity and specificity were 86.1%, and 75%, respectively.

¹⁸F-FDG-PET/CT is expensive, involves isotopic radiation, and has high false-positive rates in inflammatory processes. In addition, ¹⁸F-FDG-PET/CT has low sensitivity for detecting micrometastases in ALNs (1, 3). The mean ALN metastasis diameter of 41 patients in the upfront surgery group, considered false negatives in ¹⁸F-FDG-PET/CT results, was 4.56 mm. Micrometastases (0.2–2 mm) were detected in 13 of these patients. Its main advantage is that it is a functional imaging method that enables early detection of distant metastases (21, 22).

The mean pathologic ALN metastasis diameter was 3.73 mm in false negative AUS, 3.54 mm in false negative MRI, and 4.56 mm in false negative ¹⁸F-FDG-PET/CT in the upfront surgery group, respectively. In our and other imaging-pathologic comparative studies the mean diameter of metastatic ALNs was smaller in false negative cases of AUS, MRI, or ¹⁸F-FDG-PET/CT than the diameter of metastases that were

visible in these modalities. One study reported that the prognostic information obtained from MRI has a certain advantage over AUS, particularly when considering axillary surgery, and that MRI provides a more accurate prediction of axillary nodal burden than AUS (12). When nodal burden and false negative AUS, MRI, and ¹⁸F-FDG-PET/CT were evaluated in upfront surgery patients, two patients were pN2 on AUS, one was pN2 on MRI, and three were pN2 and two were pN3 on ¹⁸F-FDG-PET/CT. MRI and AUS were found to provide a more accurate prediction compared to ¹⁸F-FDG-PET/CT. In an earlier study, we found that the nodal burden is predictable according to the ALN SUV_{max} results, which is important when deciding between surgical or NAC treatment (23).

In a previous study, histopathologically confirmed ALN metastases were detected in 13 of 82 patients. ALN SUV_{max} showed an AUC value of 0.916, and the cut-off value of 1.1 was appropriate (24). The overall accuracy, sensitivity, and specificity of the ALN SUV_{max} cut-off value of 0.72 for the detection of ALN metastases were approximately 65.3%, 85.8%, and 77.8 %, respectively, and its positive and negative predictive values were 74.7% and 79.4%, respectively (25). In the present study, the AUC was 0.851. Riegger et al. (26) found that ¹⁸F-FDG-PET/CT was significantly more accurate than AUS for the detection of ALN metastases (p = 0.019). The sensitivity, specificity, PPV, NPV, and accuracy of ¹⁸F-FDG-PET/CT for the detection of ALN metastases in that study were 54%, 89%, 77%, 74%, and 75%, respectively. For AUS they were 38%, 78%, 54%, 65%, and 62%, respectively (26). In our study,

Table 4. Mean metastasis diameter, pN, histopathological types and luminal subtypes data of imaging modalities

		ALN (+), radiological (+) (true positive)		ALN (-), radiological (+) (false positive)		ALN (-), radiological (-) (true negative)		ALN (+), radiological (-) (false negative)		
AUS	Mean metastasis diameter, (mm) (n=236)	11.18	n=67	0	n=14	0	n=124	3.73	n=31	
	pN, (n) (n=236)	pN0: benign	0		14	n=14	124		0	
		pN1: 1–3	37		0		0		29	
		pN2: 4–9	21	n=67	0		0	n=124	2	n=31
		pN3: ≥10	9		0		0		0	
	Luminal subtypes, (n) (n=336)	A	20		4		54		10	
		B, HER2 (-)	79		10		41		14	
		B, HER2 (+)	28	n=157	2	n=24	11	n=124	1	n=31
		HER2 (+)	14		3		8		5	
		TN	16		5		10		1	
	Histopathological types, (n) (n=336)	IDC	130		20		79		24	
		ILC	13	n=157	2	n=24	9	n=124	2	n=31
		IDC + ILC	1		1		2		1	
		Others	13		1		34		4	
MRI	Metastasis diameter, (mm) (n=236)	11.52	n=67	0	n=3	0	n=135	3.54	n=31	
	pN, (n) (n=236)	pN0: benign	0		3		135		0	
		pN1: 1–3	37	n=67	0	n=3	0	n=135	29	n=31
		pN2: 4–9	21		0		0		2	
		pN3: ≥10	9		0		0		0	
	Luminal subtypes, (n) (n=336)	A	20		2		56		11	
		B, HER2 (-)	77		0		51		16	
		B, HER2 (+)	26	n=152	1	n=3	12	n=145	3	n=36
		HER2 (+)	13		0		11		6	
		TN	16		0		15		0	
	Histopathological types, (n) (n=336)	IDC	124		2		97		29	
		ILC	12	n=152	1	n=3	10	n=145	3	n=36
		IDC + ILC	2		0		3		0	
		Others	14		0		35		4	
¹⁸ F-FDG-PET/CT	Mean metastasis diameter, (mm) (n=236)	12.18	n=57	0	n=13	0	n=125	4.56	n=41	
	pN, (n) (n=236)	pN0: benign	0		13		125		0	
		pN1: 1–3	30	n=57	0	n=13	0	n=125	36	n=41
		pN2: 4–9	20		0		0		3	
		pN3: ≥10	7		0		0		2	
	Luminal subtypes, (n) (n=336)	A	17		4		54		14	
		B, HER2 (-)	67		5		46		26	
		B, HER2 (+)	26	n=138	3	n=17	10	n=131	3	n=50
		HER2 (+)	12		3		8		7	
		TN	16		2		13		0	
	Histopathological types, (n) (n=336)	IDC	116		12		87		37	
		ILC	9		3		8		6	
		IDC + ILC	0	n=138	0	n=17	3	n=131	2	n=50
		Others	13		2		33		5	

pN: Pathological Node, ALN: Axillary lymph nodes, AUS: Axillary ultrasound, mm: Millimeter, HER2: Human epidermal growth factor receptor 2, TN: Triple negative, IDC: Invasive ductal carcinoma, ILC: Invasive lobular carcinoma, MRI: Magnetic resonance imaging, ¹⁸F-FDG-PET/CT: ¹⁸F-Fluorodeoxyglucose positron emission tomography/computed tomography, n: Number

Table 5. Comparison of imaging modalities and ALN status

	Upfront surgery group (n=236)			NAC group (n=100)		Total (n=336)	
	n	ALN (+) (n)	Mean ALN metastasis diameter (mm)	n	ALN (+) (n)	n	ALN (+) (n)
AUS (+), MRI (+), 18F-FDG-PET/CT (+)	48	48	12.74	84	84	132	132
AUS (+), MRI (+), 18F-FDG-PET/CT (-)	16	13	6.6	6	3	22	16
AUS (+), MRI (-), 18F-FDG-PET/CT (-)	15	6	4.16	5	1	20	7
AUS (+), MRI (-), 18F-FDG-PET/CT (+)	2	0	0	5	2	7	2
AUS (-), MRI (+), 18F-FDG-PET/CT (+)	3	3	6	0	0	3	3
AUS (-), MRI (+), 18F-FDG-PET/CT (-)	3	3	5.16	0	0	3	3
AUS (-), MRI (-), 18F-FDG-PET/CT (+)	17	6	4.2	0	0	17	6
AUS (-), MRI (-), 18F-FDG-PET/CT (-)	132	19	3.27	0	0	132	19

ALN: Axillary lymph nodes, NAC: Neoadjuvant chemotherapy, mm: Millimeter, AUS: Axillary ultrasound, MRI: Magnetic resonance imaging, 18F-FDG-PET/CT: 18F-Fluorodeoxyglucose positron emission tomography/computed tomography, n: Number

Table 6. Data of luminal subtypes and histopathological types of false negative patients

	AUS (-), MRI (-), 18F-FDG-PET/CT (-) (n=132)			ALN (+) (false negative)	
Upfront surgery group (n=236)				n=19 (0.2-9mm) (14.3%)	
				1: 4 metastases (pN2)	
				1: 2 metastases (pN1)	
				17: 1 metastasis (pN1) (5: pN1mic)	
Luminal subtypes (n/%)	A	55	41.6	6	31.5
	B, HER2 (-)	49	37.1	9	47.3
	B, HER2 (+)	8	6.1	0	0
	HER2 (+)	11	8.3	4	21.1
	TN	9	6.8	0	0
Histopathological types (n/%)	IDC	88	66.6	14	73.6
	ILC	8	6.1	2	10.5
	IDC + ILC	2	1.5	0	0
	Others	34	25.7	3	15.7

AUS: Axillary ultrasound, MRI: Magnetic resonance imaging, 18F-FDG-PET/CT: 18F-Fluorodeoxyglucose positron emission tomography/computed tomography, ALN: Axillary lymph nodes, mm: Millimeter, pN: Pathological node, HER2: Human epidermal growth factor receptor 2, TN: Triple negative, IDC: Invasive ductal carcinoma, ILC: Invasive lobular carcinoma, n: Number

MRI and AUS had higher accuracy for showing ALN metastases compared to 18F-FDG-PET/CT (MRI, AUS, 18F-FDG-PET/CT; 85.3%, 79.1%, and 72.5%, respectively). In another study, there were no statistically significant differences between MRI and AUS

for the evaluation of ALNs (27). However, with MRI alone or AUS combined with MRI, that study found a statistically significant difference in specificity and PPV. Among the 21 MRI or 18F-FDG-PET/CT studies included in a meta-analysis, the pooled sensitivities

of MRI and ¹⁸F-FDG-PET/CT were 0.82 and 0.64, respectively, suggesting that MRI has a higher sensitivity than ¹⁸F-FDG-PET/CT for an ALN metastasis diagnosis in breast cancer patients (21). It has been reported that MRI is better at diagnosing ALN metastases in breast cancer than ¹⁸F-FDG-PET/CT, and MRI combined with US can lead to a more precise diagnosis (28). In our study, MRI was found to have higher sensitivity and specificity for showing ALN metastases compared to ¹⁸F-FDG-PET/CT (86.1%, 75% and 78%, 53%, respectively). An et al. (29) found that ¹⁸F-FDG-PET/CT for detection of ALN metastasis was not significantly different from AUS or MRI in breast cancer patients. They concluded that combining ¹⁸F-FDG-PET/CT with AUS or MRI could improve the diagnostic performance compared to ¹⁸F-FDG-PET/CT alone (29). In our study, ALNs were found to be metastatic in all patients who were reported positive in all three imaging modalities. Using multiple imaging modalities improved overall imaging diagnostic performance and increased accuracy. However, it should be noted that although all three imaging modalities were negative, we found 14.3% false negativity.

Our study had some limitations. First, we evaluated the cases retrospectively. In addition, imaging data was obtained from different imaging centers, and thus lack of standardization was inevitable. Also, AUS is an operator-dependent modality, which has poor interobserver agreement. So, it is important that an experienced breast radiologist should interpret the imaging findings using this modality. We could not show a one-to-one correspondence between histopathology and AUS, MRI, and ¹⁸F-FDG-PET/CT images. In addition, ALN status at the time of diagnosis of patients scheduled for NAC was evaluated with FNAC.

In conclusion, evaluation of ALNs with imaging modalities in a patient with newly diagnosed breast cancer is crucial. In most studies, the accuracy of AUS, MRI, and ¹⁸F-FDG-PET/CT in demonstrating ALN metastasis have been compared with each other and no clear conclusion has been reached. In our study, we found that the diagnostic performance of MRI was slightly better than AUS and ¹⁸F-FDG-PET/CT. When we used imaging modalities together, our accuracy rate was better than when we used them alone. Thus, we suggest that for accurate evaluation of ALNs, imaging modalities should be complementary rather than competitive.

Ethics Committee Approval: This study was approved by the Ethics Committee of İstanbul Haydarpaşa Numune Training and Research Hospital (no: TUEK- 771/04/2020, date: 04/05/2020).

Informed Consent: Retrospective study.

Peer-review: Externally peer-reviewed.

Authorship Contributions

Surgical and/or Medical Practices: A.A., M.G.G., S.A.A., F.A., S.G.; Concept: A.A., M.G.G.; Design: A.A., M.G.G.; Data Collection and/or Processing: A.A.; Analysis and/or Interpretation: A.A.; Literature Search: A.A., M.G.G.; Writing: A.A., M.G.G., S.A.A., S.G.

Conflict of Interest: No conflict of interest declared by the authors.

Financial Disclosure: The authors declare that this study received no financial disclosure.

References

- Hwang SO, Lee SW, Kim HJ, Kim WW, Park HY, Jung JH. The comparative study of ultrasonography, contrast-enhanced MRI, and (18)F-FDG PET/CT for detecting axillary lymph node metastasis in T1 breast cancer. *J Breast Cancer* 2013; 16: 315-321. (PMID: 24155761) [\[Crossref\]](#)
- Sohn YM, Hong IK, Han K. Role of [18F]fluorodeoxyglucose positron emission tomography-computed tomography, sonography, and sonographically guided fine-needle aspiration biopsy in the diagnosis of axillary lymph nodes in patients with breast cancer: comparison of diagnostic performance. *J Ultrasound Med* 2014; 33: 1013-1021. (PMID: 24866608) [\[Crossref\]](#)
- Marino MA, Avendano D, Zapata P, Riedl CC, Pinker K. Lymph node imaging in patients with primary breast cancer: concurrent diagnostic tools. *Oncologist* 2020; 25: e231-e242. doi: 10.1634/theoncologist. (PMID: 32043792) [\[Crossref\]](#)
- Ahn HS, Jang M, Kim SM, La Yun B, Lee SH. Usefulness of preoperative breast magnetic resonance imaging with a dedicated axillary sequence for the detection of axillary lymph node metastasis in patients with early ductal breast cancer. *Radiol Med* 2019; 124: 1220-1228. (PMID: 31422573) [\[Crossref\]](#)
- Available from: URL: https://www.nccn.org/professionals/physician_gls/pdf/breast_blocks.pdf [\[Crossref\]](#)
- Galimberti V, Cole BF, Zurrada S, Viale G, Luini A, Veronesi P, et al; International Breast Cancer Study Group Trial 23-01 investigators. Axillary dissection versus no axillary dissection in patients with sentinel-node micrometastases (IBCSG 23-01): a phase 3 randomised controlled trial. *Lancet Oncol* 2013; 14: 297-305. (PMID: 23491275) [\[Crossref\]](#)
- Giuliano AE, Ballman KV, McCall L, Beitsch PD, Brennan MB, Kelemen PR, et al. Effect of axillary dissection vs no axillary dissection on 10-year overall survival among women with invasive breast cancer and sentinel node metastasis: the ACOSOG Z0011 (Alliance) randomized clinical trial. *JAMA* 2017; 318: 918-926. (PMID: 28898379) [\[Crossref\]](#)
- Donker M, van Tienhoven G, Straver ME, Meijnen P, van de Velde CJ, Mansel RE, et al. Radiotherapy or surgery of the axilla after a positive sentinel node in breast cancer (EORTC 10981-22023 AMAROS): a randomised, multicentre, open-label, phase 3 non-inferiority trial. *Lancet Oncol* 2014; 15: 1303-1310. (PMID: 25439688) [\[Crossref\]](#)
- Jozsa F, Ahmed M, Baker R, Douek M. Is sentinel node biopsy necessary in the radiologically negative axilla in breast cancer? *Breast Cancer Res Treat* 2019; 177: 1-4. doi (PMID: 31152326) [\[Crossref\]](#)
- Reimer T, Stachs A, Nekljudova V, Loibl S, Hartmann S, Wolter K, et al. Restricted axillary staging in clinically and sonographically node-negative early invasive breast cancer (c/iT1-2) in the context of breast conserving therapy: first results following commencement of the Intergroup-Sentinel-Mamma (INSEMA) trial. *Geburtshilfe Frauenheilkd* 2017; 77: 149-157. (PMID: 28331237) [\[Crossref\]](#)
- Gentilini O, Botteri E, Dadda P, Sangalli C, Boccardo C, Peradze N, et al. Physical function of the upper limb after breast cancer surgery. Results from the SOUND (Sentinel node vs. Observation after axillary Ultrasound) trial. *Eur J Surg Oncol* 2016; 42: 685-689. (PMID: 26899941) [\[Crossref\]](#)
- Assing MA, Patel BK, Karamsadkar N, Weinfurter J, Usmani O, Kiluk JV, et al. A comparison of the diagnostic accuracy of magnetic resonance imaging to axillary ultrasound in the detection of axillary nodal metastases in newly diagnosed breast cancer. *Breast J* 2017; 23: 647-655. (PMID: 28397344) [\[Crossref\]](#)
- Sui WF, Chen X, Peng ZK, Ye J, Wu JT. The diagnosis of metastatic axillary lymph nodes of breast cancer by diffusion weighted imaging: a meta-analysis and systematic review. *World J Surg Oncol* 2016; 14: 155. (PMID: 27255520) [\[Crossref\]](#)

14. Hafiz A, Adeniji-Sofoluwe AT, Ademola AF, Obajimi MO. Sonographic evaluation of axillary lymph nodes in women with newly diagnosed breast cancer at the university college hospital Ibadan, Nigeria. *Niger Postgrad Med J* 2018; 25: 79-86. (PMID: 30027918) [\[Crossref\]](#)
15. Black D. Axillary ultrasound: for all, for none, to diagnose positive nodes, or to support avoiding sentinel lymph node biopsy altogether. *Ann Surg Oncol* 2017; 24: 64-69. (PMID: 27557827) [\[Crossref\]](#)
16. Guvenc I, Whitman GJ, Liu P, Yalniz C, Ma J, Dogan BE. Diffusion-weighted MR imaging increases diagnostic accuracy of breast MR imaging for predicting axillary metastases in breast cancer patients. *Breast J* 2019; 25: 47-55. (PMID: 30444286) [\[Crossref\]](#)
17. Cai D, Lin T, Jiang K, Sun Z. Diagnostic value of MRI combined with ultrasound for lymph node metastasis in breast cancer: Protocol for a meta-analysis. *Medicine (Baltimore)* 2019; 98: e16528. doi: 10.1097/MD.00000000000016528. (PMID: 31348268) [\[Crossref\]](#)
18. Chayakulkheeree J, Punggrassami D, Prueksadee J. Performance of breast magnetic resonance imaging in axillary nodal staging in newly diagnosed breast cancer patients. *Pol J Radiol* 2019; 84: e413-e418. doi: 10.5114/pjr.2019.89690. (PMID: 31969959) [\[Crossref\]](#)
19. Arslan G, Altintoprak KM, Yirgin IK, Atasoy MM, Celik L. Diagnostic accuracy of metastatic axillary lymph nodes in breast MRI. *Springerplus* 2016; 5: 735. (PMID: 27376003) [\[Crossref\]](#)
20. Kayadibi Y, Kılıç F, Yılmaz R, Velidedeoğlu M, Öztürk T, Tekcan DE, et al. Second look ultrasonography-guided breast biopsy with magnetic resonance imaging confirmation by intralesional contrast injection. *Eur J Breast Health* 2021; 17: 1-9. (PMID: 33796824) [\[Crossref\]](#)
21. Liang X, Yu J, Wen B, Xie J, Cai Q, Yang Q. MRI and FDG-PET/CT based assessment of axillary lymph node metastasis in early breast cancer: a meta-analysis. *Clin Radiol* 2017; 72: 295-301. (PMID: 28139203) [\[Crossref\]](#)
22. He X, Sun L, Huo Y, Shao M, Ma C. A comparative study of 18F-FDG PET/CT and ultrasonography in the diagnosis of breast cancer and axillary lymph node metastasis. *Q J Nucl Med Mol Imaging* 2017; 61: 429-437. (PMID: 25823388) [\[Crossref\]](#)
23. Aktas A, Aslayan SO, Gurleyik MG, Gungor S. Correlations of primary tumor SUVmax and axillary lymph node SUVmax with molecular subtypes of invasive breast cancer. *Indian J Surg* 2021; 1-7. [\[Crossref\]](#)
24. Mori M, Fujioka T, Katsuta L, Tsuchiya J, Kubota K, Kasahara M, et al. Diagnostic performance of time-of-flight PET/CT for evaluating nodal metastasis of the axilla in breast cancer. *Nucl Med Commun* 2019; 40: 958-964. (PMID: 31365505) [\[Crossref\]](#)
25. Jung NY, Kim SH, Kang BJ, Park SY, Chung MH. The value of primary tumor (18)F-FDG uptake on preoperative PET/CT for predicting intratumoral lymphatic invasion and axillary nodal metastasis. *Breast Cancer* 2016; 23: 712-717. (PMID: 26219608) [\[Crossref\]](#)
26. Riegger C, Koeninger A, Hartung V, Otterbach F, Kimmig R, Forsting M, et al. Comparison of the diagnostic value of FDG-PET/CT and axillary ultrasound for the detection of lymph node metastases in breast cancer patients. *Acta Radiol* 2012; 53: 1092-1098. (PMID: 23002144) [\[Crossref\]](#)
27. Abe H, Schacht D, Kulkarni K, Shimauchi A, Yamaguchi K, Sennett CA, et al. Accuracy of axillary lymph node staging in breast cancer patients: an observer-performance study comparison of MRI and ultrasound. *Acad Radiol* 2013; 20: 1399-1404. (PMID: 24119352) [\[Crossref\]](#)
28. Cai D, Lin T, Jiang K, Sun Z. Diagnostic value of MRI combined with ultrasound for lymph node metastasis in breast cancer: Protocol for a meta-analysis. *Medicine (Baltimore)* 2019; 98: e16528. doi: 10.1097/MD.00000000000016528. (PMID: 31348268) [\[Crossref\]](#)
29. An YS, Lee DH, Yoon JK, Lee SJ, Kim TH, Kang DK, Kim KS, Jung YS, Yim H. Diagnostic performance of 18F-FDG PET/CT, ultrasonography, and MRI. Detection of axillary lymph node metastasis in breast cancer patients. *Nuklearmedizin* 2014; 53: 89-94. (PMID: 24220324) [\[Crossref\]](#)